8. Osava, M. *et al.* A novel target recognition revealed by calmodulin in complex with Ca^{2+} calmodulin dependent kinase kinase. *Nature Struct. Biol.* **6,** 819–826 (1999).
9. Elhorst, B. *et al.* NMR solution structure of a complex of calmodulin with a binding peptide of the Ca^{2+} pump. *Biochemistry* **38,** 12320–12326 (1999).
10. Rhoads, A. R. & Friedberg, F. Sequence motifs for calmodulin binding. *FASEB J.* **11,** 331–339 (1997).
11. Babu, Y. S. *et al.* Three-dimensional structure of calmodulin. *Nature* **315,** 37–40 (1985).
12. Chattopadhyaya, R., Meador, W. E., Means, A. R. & Quiocho, F. A. Calmodulin structure refined at 1. 7 Å resolution. *J. Mol. Biol.* **228,** 1177–1192 (1992).
13. Zhang, M., Tanaka, T. & Ikura, M. Calcium-induced conformational transition revealed by the solution structure of the apo calmodulin. *Nature Struct. Biol.* **2,** 758–767 (1995).
14. Kuboniwa, H. *et al.* Solution structure of calcium-free calmodulin. *Nature Struct. Biol.* **2,** 768–776 (1995).
15. Finn, B. E. *et al.* Calcium-induced structural changes and domain autonomy in calmodulin. *Nature Struct. Biol.* **2,** 777–783 (1995).
16. Liu, Y., Holgrem, M., Jurman, M. E. & Yellen, G. Gated access to the pore of a voltage-dependent K^+ channel. *Neuron* **19,** 175–184 (1997).
17. del Camino, D., Holgrem, M., Liu, Y. & Yellen, G. Blocker protection in the pore of a voltage-gated K^+ channel and its structural implications. *Nature* **403,** 321–325 (2000).
18. Holmgren, M., Shin, K. S. & Yellen, G. The activation gate of a voltage-gated K^+ channel can be trapped in the open state by an intersubunit metal bridge. *Neuron* **21,** 617–621 (1998).
19. Doyle, D. A. *et al.* The structure of the potassium channel: molecular basis of K^+ conduction and selectivity. *Science* **280,** 69–77 (1998).
20. Perozo, E., Cortes, D. M. & Cuello, L. G. Structural rearrangements underlying K^+-channel activation gating. *Science* **285,** 73–78 (1999).
21. Fragioni, J. V. & Neel, B. G. Solubilization and purification of enzymatically active glutatione S-transferase (pGEX) fusion proteins. *Anal. Biochem.* **210,** 179–187 (1993).
22. Howard, A. J., Nielson, C. & Xuong, N. H. Software for a diffractometer with multiwire area detector. *Methods Enzymol.* **114,** 452–472 (1985).
23. Furey, W. B. & Swaminathan, S. PHASE-95: a program package for the processing and analysis of diffraction data from macromolecules. *Methods Enzymol.* **277,** 590–620 (1997).
24. Jones, T. A., Zou, J.-Y., Cowan, S. W. & Kjeldgaard, M. Improved methods for building protein models in electron density maps and the location of errors in these models. *Acta Crystallogr. A* **47,** 110–119 (1991).
25. Tronrud, D. E., TenEyck, L. F. & Matthews, B. W. An efficient general purpose least-squares refinement program for macromolecular structures. *Acta Crystallogr. A* **43,** 489–501 (1985).
26. Kissinger, C. R., Gehlaer, D. K. & Fogel, D. B. Rapid automated molecular replacement by evolutionary search. *Acta Crystallogr. D* **55,** 484–491 (1999).
27. Brünger, A. T. *et al.* Crystallography & NMR system: A new software suite for macromolecular structure determination. *Acta Crystallogr. D* **54,** 905–921 (1998).
28. Laskowski, R. A., MacArthur, M. W. & Thorton, J. M. PROCHECK: a program to check the stereochemical quality of protein structures. *J. Appl. Crystallogr.* **26,** 283–291 (1993).
29. Kraulis, P. J. MOLSCRIPT: a program to produce both detailed and schematic plots of protein structures. *J. Appl. Crystallogr.* **24,** 946–950 (1991).
30. Nicholls, A., Sharp, K. & Honig, B. H. Protein folding and association: insights from the interfacial and thermodynamic properties of hydrocarbons. *Proteins Struct. Funct. Genet.* **11,** 281–296 (1991).

Supplementary information is available on *Nature*'s World-Wide Web site (http://www.nature.com) or as paper copy from the London editorial office of *Nature*.

Acknowledgements

M.A.S. is a Burroughs Wellcome Career Development Awardee. This work was supported by grants from the NIH, the Muscular Dystrophy Association, and the Human Frontiers of Science Foundation. Intensity data collected at the Stanford Synchrotron Radiation Laboratory (SSRL) was carried out under the auspices of the SSRL biotechnology program, which is supported by the National Institutes of Health, National Center for Research Resources, Biomedical Technology Program, and by the Department of Energy, Office of Biological and Environmental Research.

Correspondence and requests for materials should be addressed to M.A.S. (e-mail: schumacm@ohsu.edu). Coordinates have been deposited with the Protein Data Bank under accession code 1G4Y.

erratum

Increase in greenhouse forcing inferred from the outgoing longwave radiation spectra of the Earth in 1970 and 1997

John E. Harries, Helen E. Brindley, Pretty J. Sagoo & Richard J. Bantges

Nature **410,** 355–357 (2001).

In Fig. 1a of this paper, the labels for the two curves were inadvertently switched. The grey curve represents IMG and the black curve represents IRIS. □

Increases in greenhouse forcing inferred from the outgoing longwave radiation spectra of the Earth in 1970 and 1997

John E. Harries, Helen E. Brindley, Pretty J. Sagoo & Richard J. Bantges

Space and Atmospheric Physics Group, Blackett Laboratory, Imperial College, London SW7 2BW, UK

The evolution of the Earth's climate has been extensively studied[1,2], and a strong link between increases in surface temperatures and greenhouse gases has been established[3,4]. But this relationship is complicated by several feedback processes—most importantly the hydrological cycle—that are not well understood[5–7]. Changes in the Earth's greenhouse effect can be detected from variations in the spectrum of outgoing longwave radiation[8–10], which is a measure of how the Earth cools to space and carries the imprint of the gases that are responsible for the greenhouse effect[11–13]. Here we analyse the difference between the spectra of the outgoing longwave radiation of the Earth as measured by orbiting spacecraft in 1970 and 1997. We find differences in the spectra that point to long-term changes in atmospheric CH_4, CO_2 and O_3 as well as CFC-11 and CFC-12. Our results provide direct experimental evidence for a significant increase in the Earth's greenhouse effect that is consistent with concerns over radiative forcing of climate.

Starting in October 1996, the Interferometric Monitor of Greenhouse Gases (IMG) instrument[14], on board the Japanese ADEOS satellite, produced about nine months of global observations of the spectrum of outgoing longwave radiation. Some 27 years earlier, NASA had flown a similar instrument (IRIS—Infrared Interferometric Spectrometer[15]) on the Nimbus 4 spacecraft, between April 1970 and January 1971. Details of the performance of the two instruments are given in Table 1. Although these two experiments were on board separate spacecraft almost 30 years apart, the existence of the two data sets allows the examination of the outgoing longwave radiation spectra to detect whether any significant change had occurred between the two measurements. Comparing averaged spectra for the same region, allowing for the different spatial and spectral resolutions of the two instruments, reveals that they are extremely similar and highly reproducible. Nevertheless, on closer inspection, informative differences are observed.

To illustrate this, Fig. 1a shows an averaged IRIS cloud-cleared brightness temperature spectrum superposed on an averaged IMG cloud-cleared spectrum, for the same three-month period (April–June) and a central Pacific area (latitude 10° N–10° S, longitude 130° W–180° W) for the range 710–1,400 cm^{-1}. The spectral resolution of the IMG data has been degraded to match that of IRIS, instrument field-of-view effects have been taken into account, and land/island areas have been masked out. For cloud clearing, a two-step approach was used[16]. Figure 1b shows three curves: upper, the difference IMG–IRIS taken directly from Fig. 1a; middle, a theoretical difference spectrum, corresponding to conditions for the central Pacific; and lower, the observed difference spectrum for a 'near-global' case (60° N–60° S) for the same period, for comparison. The curves in Fig. 1b are displaced by 5 K from one another. Figure 1c shows the component of the simulated spectrum that includes only the effect of trace-gas changes between 1970 and 1997 (omitting temperature and humidity changes), to aid interpretation.

The agreement between the upper and middle curves of Fig. 1b is very good. This result, given that the IMG and IRIS data were recorded using two separate spectrometers, 27 years apart, and that the simulation is completely independent of IRIS/IMG observations, gives confidence in the quality of the data. The internal consistency of the data is further illustrated by the inclusion of the bottom, quasi-global result. Despite the fact that the averages in the top and bottom curves contain very different numbers of spectra, the consistency between these results is notable: the major features of the observed difference spectra appear consistently in all the difference spectra we have studied.

Our interpretation of Fig. 1 is as follows. We consider first the sharp spectral features. A negative-going brightness temperature difference is observed on the edge of the CO_2 ν_2 band, between 710 and 740 cm^{-1}, in accord with the known increase in atmospheric CO_2 concentrations between 1970 and 1997[1]. The O_3 band centred at about 1,060 cm^{-1} also shows a negative-going difference from the background window signal, which can be attributed to the known changes in ozone[17] and in temperature[18]. A strong, negative Q-branch is observed at 1,304 cm^{-1} in the CH_4 band, due mainly to increases in tropospheric CH_4 concentrations in the period between the observations, which causes emission from higher, colder layers of the troposphere. Negative-going lines due to ν_2-band H_2O absorption are seen between 1,200 and 1,400 cm^{-1}. There is also evidence of weak features due to CO_2, CFC-11 and CFC-12 in the 700–1,000 cm^{-1} range.

We now consider the background difference spectrum in the two window regions on either side of the O_3 band. The window difference spectrum could be influenced by changes in surface temperature (assuming constant oceanic emissivity), humidity of the lower troposphere, aerosol content, or cloud amount and type. Consistently, the difference in the 1,100–1,200 cm^{-1} window is close to zero (within ±1 K), while the difference in the 800–1,000 cm^{-1} region is positive, and lies between about 1 and 2 K. It is important not to over-interpret the observations to an accuracy that is not justified by the errors (see below), nor to lose sight of our principal result, which is the observation of the sharp spectral features discussed in the preceding paragraph. Nevertheless, we believe that this reproducible difference between the windows is consistent with small residual amounts of ice cloud in both averaged spectra, possibly exacerbated by the different fields of view of the two instruments: we discuss this further below.

The simulations shown in Fig. 1b and c were calculated as follows. Profiles of atmospheric temperature and water vapour were extracted covering the same region and three-month time periods from the NCEP (National Centers for Environmental Prediction, Washington) reanalysis project[19]. Stratospheric ozone changes were estimated using measured trends[20] extrapolated back to 1970, whereas tropospheric ozone changes were calculated using a three-dimensional chemical transport model, forced by realistic emission scenarios[21]. Remaining gaseous concentrations were taken from the relevant IPCC values for CO_2, CH_4, N_2O, CFC-11 and CFC-12, in 1970 and 1997. The MODTRAN3 code[22] was used to calculate the expected radiance spectra in 1970 and 1997.

All the principal features due to changes in CO_2, CH_4, O_3, temperature and humidity are well modelled, as are the small

Table 1 IMG and IRIS instrument characteristics

Characteristic	IMG	IRIS
Spectral range (cm^{-1})	600–3,000	400–1,600
Spatial field of view	8 km × 8 km	100 km × 100 km
Spectral resolution (cm^{-1})	0.10–0.25	2.8
Total radiometric uncertainty ($mW\,m^{-2}\,sr^{-1}$ per cm^{-1})	±0.23	±(0.5†–1.0‡)
Equivalent brightness temperature uncertainty* (K)	±0.15	±(0.3†–0.6‡)

* Defined at 900 cm^{-1} for a brightness temperature of 290 K.
† In centre of band.
‡ Towards edge of band.

changes due to the chlorofluorocarbons (for example, at 850 and 920 cm^{-1}) and weak CO_2 bands (for example, at 795 cm^{-1}). We note that the main features of the observed difference spectrum can only be reproduced by including the long-term changes in CH_4, CO_2, O_3 and the chlorofluorocarbons: inter-annual and short-term variability is not sufficient.

We must consider, however, whether any aspect of the observed difference spectra could be caused by instrumental, or other, artefacts. We have considered three: the accuracy and precision of the spectra; possible causes of differential window signals; and inter-annual variability.

First, we have examined the central issue of the accuracy and precision of the two data sets, and whether our analysis is justified on this count. We believe it is, for the following reasons. (1) We have reported above the agreement between the observed difference spectra and simulated spectra, which are calculated quite independently from basic knowledge of the atmospheric state. (2) We have derived difference spectra over a wide variety of regions and times (including the east and west Pacific, Atlantic, and Indian oceans) and see consistency in the principal absorption features. (3) Random error is reduced by averaging: in the extreme case in which all the error in Table 1 is assumed to be random, we obtain a value of ±0.058 K for the central Pacific difference spectra. (4) Absolute accuracy is potentially a more serious issue: if all the error quoted in Table 1 were systematic, this would indicate a maximum absolute peak–peak error for the combined data of about 0.45 K at the centre of the IRIS/IMG pass bands, increasing to about 0.75 K at the edges. Such errors of absolute calibration vary slowly with wavenumber, and could produce small 'ghosts' at the positions of the observed spectral features, though these are very unlikely to be significant. Slowly varying systematic errors[23] may also contribute to the differential window signal, but only at this same level of <0.45 K. (5) Normalization of each averaged spectrum to the intensity at one selected wavenumber indicates no significant multiplicative error between IMG and IRIS above the 0.5 K level. (6) Examination of the data shows that neither spatial nor temporal sampling is seriously biased. We conclude that the main features of the observed spectra cannot be accounted for by instrument errors, but that the absolute calibration of the difference spectra might be in error by up to about 0.5 to 0.75 K peak–peak.

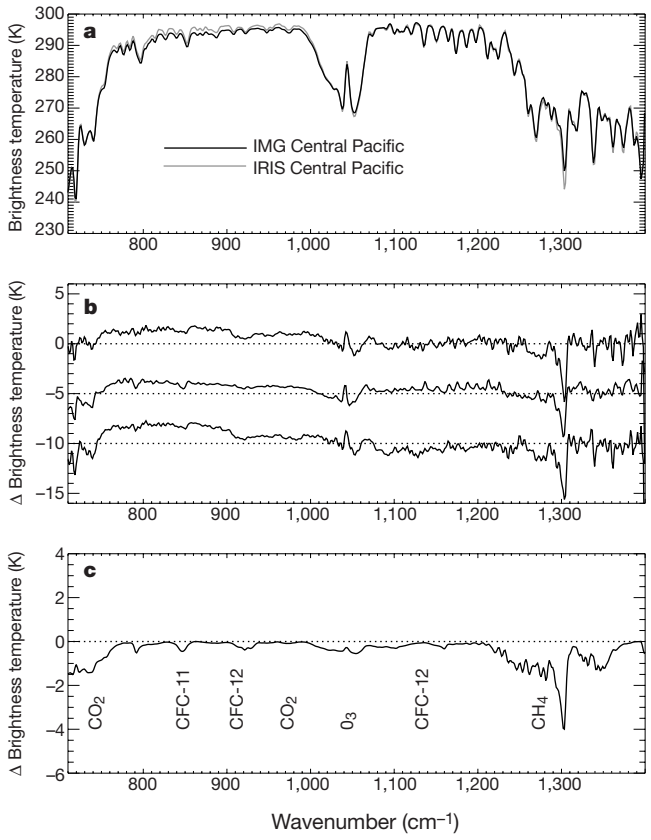

Figure 1 Examples of IRIS and IMG observed and simulated spectra for a three-month average (April–June) over selected regions. **a,** Observed IRIS and IMG clear sky brightness temperature spectra for the central Pacific (10° N–10° S, 130° W–180° W). **b,** Top, observed difference spectrum taken from **a**; middle, simulated central Pacific difference spectrum, displaced by –5 K; bottom, observed difference spectrum for 'near-global' case (60° N–60° S), displaced by –10 K. **c,** Component of simulated spectrum due to trace-gas changes only. 'Brightness temperature' on the ordinate indicates equivalent blackbody brightness temperature.

Second, we have considered the observed differences in the two window background regions, and the influence of the different fields of view of the two instruments. (We point out that this influences only the background levels: we have averaged differing numbers of IRIS and IMG spectra to show that the main features in the difference spectrum due to greenhouse gases are not dependent on the fields of view of the two instruments). However, broad-band difference signals could occur if aerosol or cloud 'contamination' remains in the notionally clear fields of view. Using available aerosol data[24], we have shown for typical conditions that aerosol absorption is unlikely to be a significant source of error (<0.1 K). However, recent work[25] has shown that ice cloud, particularly if composed of small crystals, does exhibit stronger absorption in the 800–1,000 cm^{-1} than the 1,100–1,200 cm^{-1} window. It is quite possible that small residual amounts of ice cloud absorption remain in both sets of data. Owing to the larger field of view, the IRIS spectra have a much higher probability of being contaminated than their IMG counterparts. The observed 1 K or so enhancement of the 800–1,000 cm^{-1} difference signal would be consistent with this, and could also arise from a change in the mean cirrus microphysical properties. We cannot separate these two effects, but we do conclude that the observed window difference spectra strongly indicate an effect involving residual small ice crystal effects, incompletely cleared from the data. R.J.B. has performed further calculations, following on earlier work[26], which confirm that window difference spectra of the magnitude observed can easily arise from small changes in amount, size or shape of small ice crystals: these studies also indicate that the difference spectrum should be larger below about 920 cm^{-1}, which is consistent with the observed data, especially the global case (Fig. 1b). Further work on these and other cloud effects in the data will be performed separately: for the present, we believe we have demonstrated a sufficient understanding of the observations to give confidence to the principal findings of this work regarding changes in radiative forcing due to CH_4, CO_2, O_3 and the chlorofluorocarbons.

Third, we must also take into account inter-annual variability as a possible cause of the observed difference spectra. In the window region, the brightness temperature difference is strongly modulated by short-term fluctuations, such as inter-annual variability (specific concern involves the 1997 warm El Niño/Southern Oscillation, ENSO, event). Our studies show that, while this could account for an uncertainty of about 1 K in the position of the zero line in the spatially and temporally averaged difference spectra used, it could not account for the sharp spectral features observed, nor the differential window signal just discussed.

The results presented here provide (to our knowledge) the first experimental observation of changes in the Earth's outgoing long-wave radiation spectrum, and therefore the greenhouse effect: previous studies have been largely limited to theoretical simulations because of the paucity of data. We intend to examine the temporal and spatial variation of the difference spectra, and will include cloudy and all sky data. Future measurements by an IRIS-type

instrument that combines high accuracy and a narrow field of view are a priority for climate research. □

Methods

Reduction of IMG to IRIS spectral resolution and solid-angle correction

Before any further analysis, the IMG data were smoothed to match the IRIS resolution. In addition, the wavenumber scale in the two instruments is slightly different, owing to differing solid angles within the instruments[27]. An empirically derived multiplicative factor of 0.9995 was applied to the IRIS wavenumber scale. Our work indicates that this process needs to be performed extremely accurately in order to avoid artefacts appearing in the difference spectrum.

Cloud clearing and spatial resolution

Cloud clearing was achieved in two steps[16]. First, for each spectrum, the brightness temperature at 1,126.6 cm^{-1} (surface to top of atmosphere transmittance $\approx$ 0.94) was compared to the underlying sea surface temperature taken from NCEP for the same location and time. If the difference exceeded a set threshold, the spectrum was rejected as being cloud-contaminated. The threshold for both IMG and IRIS was set at 6 K. This value was found by testing the variation of the standard deviation of the spectra with the threshold value.

The remaining spectra were subjected to a second filtering, to try to remove any residual spectral effects of cirrus clouds. The brightness temperature difference between two wavenumbers (909.8 and 1,250.4 cm^{-1}) was compared with a threshold value[16]. The threshold value was chosen as before, by noting the temperature difference at which the standard deviation of the set of IRIS, or IMG, spectra fell to a near-constant value. A value of 8 K was used for IRIS spectra and 7 K for IMG. More severe cloud-clearing thresholds led to either all IRIS spectra being rejected as contaminated, or insufficient numbers of IMG spectra being retained to give the requisite spatial and temporal coverage.

Numbers of retained spectra in Fig. 1

The numbers of spectra retained and used in averaging to produce Fig. 1, after cloud clearance, were as follows. Global: IMG, 4,061; IRIS, 529. Central Pacific: IMG, 213; IRIS, 28.

Random and absolute errors

The total uncertainty of IRIS and IMG are quoted in Table 1. To examine the random and absolute components of this, we have taken the quoted errors to represent either the maximum random error (for example, caused by noise in the detector or electronics system) or the maximum systematic error (for example, multiplicative or additive error, such as absolute errors in the transmission or reflectivity of optical components such as filters and mirrors, or the temperature or emissivity of the blackbody targets used to calibrate the instruments, or an offset due to vignetting in the field of view). Such errors would typically be slowly varying with wavenumber.

For the random error, we have divided the errors quoted in Table 1 by the square root of the number of spectra left in each cloud-cleared average, and combined IMG and IRIS errors in a root-mean-square sense. The error in the difference spectrum of Fig. 1 amounts to $\pm$0.058 K. For systematic error, from Table 1 the maximum peak–peak error that could arise, and which would not be reduced by averaging, would be 0.45 K in the band centre and 0.75 K towards the edge of the band.

We note that multiplicative errors of absolute calibration as described above could produce sharp features in a difference spectrum, but that these would not exceed the quoted peak–peak error. Thus we conclude that the maximum systematic error, slowly varying across the spectrum, is probably $\leq$0.5 K.

Spectral range used in comparison

The upper limit of 1,400 cm^{-1} used in this analysis was based on the useful signal to noise ratio of IRIS; the lower limit of 710 cm^{-1} was based on the recommendations of the IMG Science Working Group.

Received 17 May 2000; accepted 15 January 2001.

1. Houghton, J., Jenkins, G. & Ephraums, J. (eds) *Climate Change: The IPCC Scientific Assessment* (Cambridge Univ. Press, Cambridge, 1990).
2. Houghton, J. *et al.* (eds) *Climate Change 1995: The Science of Climate Change* (Cambridge Univ. Press, Cambridge, 1995).
3. Mitchell, J., Johns, T., Gregory, J. & Tett, S. Climate response to increasing levels of greenhouse gases and sulphate aerosols. *Nature* **376,** 501–505 (1995).
4. Tett, S., Stott, P., Allen, M., Ingram, W. & Mitchell, J. Causes of twentieth century temperature change near the Earth's surface. *Nature* **399,** 569–575 (1999).
5. Cess, R. *et al.* Interpretation of cloud-climate feedback predicted by 14 atmospheric general circulation models. *Science* **245,** 513–516 (1989).
6. Rind, D. *et al.* Positive water vapour feedback in climate models confirmed by satellite observations. *Nature* **349,** 500–503 (1991).
7. Lindzen, R. Some coolness regarding global warming. *Bull. Am. Meteorol. Soc.* **71,** 288–299 (1990).
8. Goody, R., Haskins, R., Abdou, W. & Chen, L. Detection of climate forcing using emission spectra. *Earth Observ. Remote Sensing* **13,** 713–722 (1995).
9. Harries, J., Brindley, H. & Geer, A. Climate variability and trends from operational satellite spectral data. *Geophys. Res. Lett.* **25,** 3975–3978 (1998).
10. Goody, R., Anderson, J. & North, G. Testing climate models: an approach. *Bull. Am. Meteorol. Soc.* **79,** 2541–2549 (1998).
11. Slingo, A. & Webb, M. The spectral signature of global warming. *Q. J. R. Meteorol. Soc.* **123,** 293–307 (1996).
12. Clough, S., Iacono, M. & Moncet, J.-L. Line-by-line calculations of atmospheric fluxes and cooling rates: Application to water vapor. *J. Geophys. Res.* **97,** 15761–15785 (1992).
13. Clough, S. & Iacono, M. Line-by-line calculation of atmospheric fluxes and cooling rates: 2. Application to carbon dioxide, methane, nitrous oxide and the halocarbons. *J. Geophys. Res.* **100,** 16519–16535 (1995).
14. IMG mission operation and verification committee. *Interferometric Monitor for Greenhouse Gases* (ed. Kobayashi, H.) (IMG Project Technical Report, Central Research Institute of Electric Power Industry (CRIEPI), Komae Research Laboratory, Komae-shi, Tokyo, 1999).
15. Hanel, R., Schlachman, B., Rogers, D. & Vanous, D. Nimbus 4 Michelson interferometer. *Appl. Opt.* **10,** 1376–1382 (1971).
16. Strabala, K., Ackerman, S. & Menzel, W. Cloud properties inferred from 8-12 μm data. *J. Appl. Meteorol.* **33,** 212–229 (1994).
17. *Scientific Assessment of Ozone Depletion: 1998* Ch. 4 (Report No. 44, Global Ozone Research and Monitoring Project, World Meteorological Organization, Geneva, 1999).
18. Oort, A. & Liu, H. Upper air temperature trends over the globe. 1958-1989. *J. Clim.* **6,** 292–307 (1993).
19. Kalnay, E. *et al.* The NCEP/NCAR 40-year re-analysis project. *Bull. Am. Meteorol. Soc.* **77,** 437–471 (1996).
20. Randel, W. & Wu, F. A stratospheric ozone trends data set for global modeling studies. *Geophys. Res. Lett.* **26,** 3089–3092 (1999).
21. Olivier, J. *et al. Description of EDGAR Version 2.0: A Set of Global Emission Inventories of Greenhouse Gases and Ozone-depleting Substances for all Anthropogenic and Most Natural Sources on a Per Country Basis and on a 1 Deg x 1 Deg Grid* (RIVM Report No. 771060 002 and TNO-MEP Report No. R96/119, National Institute of Public Health and the Environment, Bilthoven, The Netherlands, 1996).
22. Berk, A., Bernstein, L. & Robertson, D. *MODTRAN: a Moderate Resolution Model for LOWTRAN 7* (AFGL-TR-88-0177, US Air Force Geophysics Laboratory, Hanscom Air Force Base, Massachusetts, 1989).
23. Hanel, R. *et al.* The Nimbus 4 infrared spectroscopy experiment 1. Calibrated thermal emission spectra. *J. Geophys. Res.* **77,** 2629–2641 (1972).
24. Shettle, E. P. in *Atmospheric Propagation in the UV, Visible, IR and MM-wave Region and Related System Aspects* 15-1–15-12 (AGARD-CP-454, Air Force Geophysics Lab., Bedford, Massachusetts, 1990).
25. Ackerman, S., Smith, W., Spinhirne, J. & Revercomb, H. The 27-28 October 1986 FIRE IFO cirrus case study: spectral properties of cirrus cloud in the 8-12 um window. *Mon. Weath. Rev.* **118,** 2377–2388 (1990).
26. Bantges, R., Russell, J. & Haigh, J. Cirrus cloud top-of-atmosphere radiance spectra in the thermal infrared. *J. Quant. Spectrosc. Radiat. Transfer* **63,** 487–498 (1999).
27. Chamberlain, J. *The Principles of Interferometric Spectroscopy* (Wiley, Chichester, 1979).

Acknowledgements

We thank L. Chen and R. Goody for providing access to IRIS data, and S. Taguchi and H. Kobayashi for providing access to IMG data.

Correspondence and requests for materials should be addressed to J.E.H. (e-mail: j.harries@ic.ac.uk).

Fossil evidence of water lilies (Nymphaeales) in the Early Cretaceous

Else Marie Friis*, Kaj Raunsgaard Pedersen† & Peter R. Crane‡

* *Department of Palaeobotany, Swedish Museum of Natural History, Box 50007, SE-104 05 Stockholm, Sweden*
† *Department of Geology, University of Aarhus, Universitetsparken, DK-8000 Århus C, Denmark*
‡ *Royal Botanical Gardens, Kew, Richmond, Surrey TW9 3AB, UK*

Phylogenetic analyses have identified the water lilies (Nymphaeales: Cabombaceae and Nymphaeaceae), together with four other small groups of flowering plants (the 'ANITA clades': Amborellaceae, Illiciales, Trimeniaceae, Austrobaileyaceae), as the first diverging lineages from the main branch of the angiosperm phylogenetic tree[1–4], but evidence of these groups in the earliest phases of the angiosperm fossil record has remained elusive. Here we report the earliest unequivocal evidence, based